

PARAMETRIC ANALYSIS OF CONCRETE RESPONSE UNDER HIGH TEMPERATURES VIA A THERMO-HYDRIC NUMERICAL MODEL

Thaís Rossi Lopes Soares^a, Michèle Cristina Resende Farage^{a,b}, Flávia de Souza Bastos^{a,b}
and Norbert Renault^c

^a*Programa de Pós Graduação em Modelagem Computacional, Universidade Federal de Juiz de Fora, Rua José Lourenço Kelmer, S/n - Martelos, Juiz de Fora - MG, Brasil, ppg.modelagemcomputacional@ufjf.edu.br, <http://www.ufjf.br/pgmc>*

^b*Departamento de Mecânica Aplicada e Computacional, Universidade Federal de Juiz de Fora, Rua José Lourenço Kelmer, S/n - Martelos, Juiz de Fora - MG, Brasil, depto.mac@ufjf.edu.br, <http://www.ufjf.br/mac>*

^c*L2MGC - Laboratoire de Mécanique et Matériaux du Génie Civil, Université de Cergy-Pontoise, 5 Mail Gay-Lussac, Neuville-sur-Oise, 95031 Cergy-Pontoise cedex, norbert.renault@u-cergy.fr, <https://www.u-cergy.fr/fr/laboratoires/labo-l2mgc.html>*

Keywords: Concrete, High temperatures, Material performance, Computational modeling, Heat transfer, Mass transfer.

Abstract. High temperatures are amongst the most critical situations in which concrete may be exposed. For safety purposes, it is, therefore, important to understand and estimate the consequences of that action on the structural integrity of concrete. The mechanical degradation suffered by a concrete structure due to high temperatures is related to energy and mass transport in a porous medium. Hence, to describe a realistic behavior of concrete undergoing thermal loading, a model shall take into account these phenomena. In this study, numerical simulations of the hygrothermal behavior of concrete specimen subjected to high temperature conditions were performed through a transient and nonlinear model, implemented in the Cast3M code. A parametric analysis was used to describe which parameters influenced more the model's performance: thermal conductivity, permeability, porosity or saturation.

1 INTRODUCTION

The use of concrete in construction presents many advantages in relation to other materials due to its mechanical performance, early strength increase, rheology of fresh concrete, compactness and durability (Mehta and Monteiro, 2006). To an extent, that last characteristic is related to deformations in concrete (Chen et al., 2010), and there exist two kinds of deformation in concrete: one kind due to external loads and other caused by temperature and moisture content variation, like shrinkage and creep. Therefore, it is important to study the effect of environmental conditions. And among them all, temperature variation is one of the most common ambient actions. Under certain situations where the concrete is exposed to high temperature (for example, caused by fires or by accidental situations in nuclear power plants), its behavior is very complex and influences the global performance of a structure during heating, impacting on the safety of people. Hence the necessity to carry studies related to this subject. Several non-linear phenomena occur in concrete when temperatures higher than ambient ones are reached: Heat conduction, vapor diffusion, liquid water flow caused by pressure gradients, capillary effects and adsorbed water content gradients, as well as latent heat transfer due to water phase change inside the pores (Gawin et al., 1999). When undergoing thermal loads, cracking and spalling are important points that relates to thermal-mechanical and hygro-thermal factors (Khoury, 2000; Gawin et al., 2006).

This work carries a study about a model that allows the analyses of concrete hygrothermal behavior when subjected to high temperature loads: the temperature distribution, the modifications and the damage caused by heating. The model used here was developed by the French Atomic Research Center (CEA, France) by Sercombe et al. (2001) and improved at L2MGC (Laboratoire de Mécanique et Matériaux du Génie Civil, Université de Cergy-Pontoise) by de Morais et al. (2006) in which the model was verified using a concrete formulation proposed by Kanema et al. (2005). The mathematical model was discretized and implemented in the Cast3M code, an open source software developed at CEA.

2 CONCRETE UNDER HIGH TEMPERATURES

2.1 General aspects

The proposed work intends to evaluate the degradation of concrete structures when exposed to aggressive environments. Hence, it will be considered evolution of microscopic material properties due to exposure to heat and moisture loads. In this way, it is possible to account the influence of the material microstructure on the overall behavior of the structure.

2.2 Physical and chemical phenomena in heated concrete

Exposition to increasing temperatures may induce complicated phenomena in concrete, then predicting its behavior can become even more difficult due to its heterogeneity. Particularly, simply taking in account thermal properties is not enough to satisfactorily describe its performance. Thus, it is necessary to consider fluid flow, energy exchange, and the hydration-dehydration phenomenon. Moreover, heating can also result in strong alterations in the concrete microstructure, and those may lead to modifications in its mechanical and transport properties. The spalling is an important phenomenon which is observed at the concrete when exposed to increasing temperature. It can be defined as the detachment of concrete fragments from the surface exposed to heating. According to Ferreira et al. (2014), it may seriously damage the integrity of the entire structure by direct exposure of structural steel to fire, increasing the risk

of buckling under compression, the loss of the isolation property and other consequences. This phenomenon may be explained as the result of two mechanisms, as reported by [Mindeguia et al. \(2010\)](#):

- The thermo-mechanical process is characterized by high temperature gradients, principally in the first centimeters of the exposed surface. Mainly, those gradients are results of rapid heating, such as accidental fires, and lead to high compressive stresses near the exposed surface. Then, those stresses may locally exceed the concrete compressive strength and cause the ejection of pieces.
- The hygro-thermal process is associated with the movement of fluids in the porous medium, which may cause high pore pressure. When concrete is exposed to high temperatures, the water present in the pores as free or absorbed water begins to evaporate. Part of this water vapor migrates to inner and colder zones of the concrete, then begins to condense and progressively creates an obstruction of humidity ("moisture clog") near the exposed surface. The moisture clog is considered a region with high water content, which prevents fluid flow from heated to cold areas, hence increasing pore pressure. These pressures may locally exceed the concrete tensile strength and result in the occurrence of spalling.

2.3 Hygrothermal coupling

Several phenomena such as heat conduction, vapor diffusion, liquid water flow due to pressure gradients and capillary effects, dehydration and vaporization occur in concrete structures subjected to high temperature loads. Thus, it is necessary to apply a model capable of describing the coupled transfers of heat and humidity in the heated concrete to better analyze the behavior of these type of structures.

The model adopted here describes the coupled transport of humidity and mass in concrete under high temperature, and it is based in porous media theory and some simplifying assumptions. The model governing equations are obtained using the law of mass and energy conservation, and the chosen state variables are: temperature and saturation.

3 MATHEMATICAL MODEL

In the mathematical formulation, the concrete is treated at a macroscopic level, as a porous, homogeneous, unsaturated and isotropic multiphase system consisting of solid (index s), liquid (index l) and gas phases (index v). The solid skeleton which deformation is disregarded, is composed of various chemical compounds and chemically bounded water. The liquid phase contain free liquid water in pores and adsorbed water physically bound to the surface of solid skeleton. Since chemically bounded water is assumed to be initially released as liquid water, the dehydrated water is also considered as part of liquid phase. The gas phase consists only of water vapor, and it is assumed to behave as an ideal gas.

The system evolution is considered to be very slow. Therefore, the state of the porous medium is assumed to be quasi-static. The phenomena of hysteresis from sorption curves are not taken into account. Hence, saturation (S_l) and humidity (h_r) are considered to be equal. The hydric transformations in concrete while increasing its temperature are defined as two-phase changes: the transformation of chemically bounded water in liquid water, caused by dehydration of the solid phase and the transformation of liquid water in vapor. Lastly, the laws of heat conduction and mass flow are uncoupled.

3.1 Governing equations

The model consists of two governing equations defining the conservation of fluid mass (i.e., vapor and liquid) and energy. The mass conservation is given by the balance equation of each fluid phase: liquid and vapor.

$$\frac{\partial m_i}{\partial t} = -\nabla \cdot \vec{J}_i + q_i \quad (1)$$

where $i = l, v$ represents the liquid or the vapor phase; m_i is the mass content per volume unit of the phase; $\nabla = \frac{\partial}{\partial x} \hat{i} + \frac{\partial}{\partial y} \hat{j} + \frac{\partial}{\partial z} \hat{k}$, presented here in cartesian coordinates, is the differential operator for vector differential calculus; $\vec{J}_i = m_i \vec{v}_i$ where \vec{v}_i is the velocity of the phase; q_i is the variation in mass due to a source. The mass content per volume unit (m_i) is expressed according to Eq.(2).

$$m_i = \phi \rho_i S_i \quad (2)$$

where ϕ , ρ_i and S_i are the porosity of the media, the density and the saturation of the phase, respectively.

In a porous media, the fluid flow may be described by Darcy's Law (Eq.(3)) when gravity effects and the material anisotropy are disregarded.

$$\vec{J}_i = -\rho_i \frac{K_i k_{ri}(S_i)}{\eta_i} \nabla(P_i), \quad (3)$$

where J_i represent liquid or vapor flow, K_i the intrinsic permeability of each phase, k_{ri} the relative permeability of the phase, η_i the viscosity and P_i , the pressure.

The modeling is based in the existence of an equilibrium between liquid and vapor water. Since the media is partially saturated and both fluid phases coexist, this hypothesis is suitable. Therefore, the pressures of liquid water (P_l) and vapor (P_v) may be related using Kelvin's equation given by Eq. (4).

$$P_l = P_{vs}(T) + \rho_l(T) \frac{RT}{M_v} \ln \frac{P_v}{P_{vs}(T)} \quad (4)$$

where R represents the ideal gas constant, T the temperature, M_v is the molar mass of water vapor and P_{vs} is the water vapor saturation pressure.

Since $S_l + S_v = 1$, it is possible to write the saturation of vapor as a function of liquid water saturation. Then, the model takes two unknowns: temperature and liquid water saturation. The combination of both mass conservation equations, the expression of flow given by Darcy's law (Eq. (3)) and Kelvin's equation (Eq. (4)), gives Eq. (5), which represents the water mechanisms:

$$\phi(d)(\rho_l(T) - \rho_v(T)) \frac{\partial S_l}{\partial t} + \phi S_l \frac{\partial \rho_l}{\partial t} = \nabla [D_h(S_l, T) \nabla S_l] + \frac{\partial d}{\partial t} \quad (5)$$

where d represents water mass generated by dehydration and D_h is the hydraulic conductivity, expressed as:

$$D_h(S_l, T) = \left[\rho_l(T) \frac{K_l(T) k_{rl}(S_l)}{\eta_l(T)} \frac{\rho_l(T)}{\rho_v(T)} + \rho_v(T) \frac{K_v(T) k_{rv}(S_v)}{\eta_v(T)} \right] \cdot P_{vs}. \quad (6)$$

The equation of energy conservation is obtained associating the equation of entropy conservation equation for a rigid porous medium, composed by three phases (solid, liquid and vapor)

in local thermodynamic equilibrium, with the expression of heat flux given by Fourier's law (see Eq. (7)).

$$c(S_l, T) \frac{\partial T}{\partial t} = \nabla \cdot (\lambda(T) \nabla T) - L_{l \rightarrow v}(T) \mu_{l \rightarrow v} + L_{s \rightarrow l}(T) \frac{\partial d}{\partial t} \quad (7)$$

where λ is the thermal conductivity, L is the latent heat of phase change, $\mu_{l \rightarrow v}$ represents the rate of fluid mass change from liquid phase to gaseous phase, $\partial d / \partial t$ is the kinetics of dehydration and $c(S_l, d)$ is the volumetric heat capacity of concrete, that is given by Eq. (8):

$$c(S_l, T) = \rho_s C_s + \phi \rho_l(T) S_l C_l + (d_0 - d) C_u \quad (8)$$

where ρ_s and ρ_l are the densities of the solid part of concrete and of the liquid water; C_s , C_l and C_u are the specific heat capacity of solid part, free water and chemically bound water, respectively; and d_0 and d are the initial mass of chemically bound water and the mass of water generated by dehydration, respectively.

4 MATERIAL PARAMETERS AND CONSTITUTIVE EQUATIONS

In this section, the evolution of different material parameters and functions, such as quantity of water generated by dehydration, porosity, intrinsic and relative permeability, thermal capacity and conductivity for the solid skeleton, and enthalpy of vaporization and dehydration, are defined regarding temperature and liquid saturation. They are expressed in Table 1 and Table 2, where m_c and m_g are the mass of cement and granulate, respectively.

Data	Value	Auxiliary parameters	Unit
Liquid water density	$\rho_l = 314.4 + 685.6 \left[1 - \left(\frac{T}{374.14} \right)^{0.55} \right]$	-	kg/m ³
Vapor water density	$\rho_v = \frac{P_{vs} M_v}{R(T + 273.15)}$	$R = 8.314(J/mol/K)$ $M_v = 0.018(kg/mol)$	kg/m ³
Liquid water viscosity	$\eta_l = 2.414 \times 10^{-5} \times e^{\frac{570.58058}{T+133.15}}$	-	kg/m/s
Vapor water viscosity	$\eta_v = (3.85 \times 10^{-8} \times T) + 10^{-5}$	-	kg/m/s
Liquid intrinsic permeability	$K_l = K_{l0} \times e^{0.126d}$	-	-
Vapor water intrinsic permeability	$K_v = K_{v0} \times e^{0.126d}$	-	-
Liquid relative permeability	$k_{rl}(S_l) = \sqrt{S_l} \times \left[1 - \left(1 - S_l^{1/m} \right)^m \right]^2$	$m = 0.5$	-
Vapor relative permeability	$k_{rv}(S_l) = \sqrt{1 - S_l} \times \left[1 - \left(1 - S_l \right)^m \right]^{2m}$	$m = 0.5$	-
Vapor saturation pressure	$P_{vs} = P_0 \times \exp \left[\frac{40500}{R} \left(\frac{T-100}{373.15(T+273.15)} \right) \right]$	$R = 8.314(J/mol/K)$ $P_0 = 101325(Pa)$	Pa
Thermal conductivity	$\lambda = 1.36 - 0.136 \left(\frac{T}{100} \right) + 0.0057 \left(\frac{T}{100} \right)^2$	-	W/mK
Dehydration latent heat	$L_{s \rightarrow l} 2500 \times 10^3$	-	(kJ/kg)
Vaporization latent heat	$L_{l \rightarrow v} = \frac{2450.2502 - 6.433949 \times T}{1 - 0.0019057413 \times T - 7.0023846 \times 10^{-7} \times T^2}$	-	(kJ/kg)
Qty. of dehydrated water	$d = 0, 136 (T - 60) \text{ for } T > 60$	-	kg/m ³
Porosity	$\phi(d) = \phi_0 + \frac{d}{\rho_{hid}}$	-	-

Table 1: Evolution of model parameters in function of temperature or liquid saturation (T in °C).

5 PARAMETRIC ANALYSIS

5.1 Introduction

Cast3M is an open source code developed by the French Atomic Research Center (CEA) in France. The solver enables the user to resolve partial differential equations through the

Material	Cement (C_c)	Aggregate (C_g)	Free water (C_l)	Bound water (C_u)	Solid phase (C_s)
Specific heat($J/kg^{\circ}C$)	750	800	4184	3760	$\frac{C_c m_c + C_g m_g}{m_c + m_g}$

Table 2: Specific heat

finite element method so that the user can adapt and incorporate models on it. The language employed is based on object-oriented programming and named GIBIANE, and the objects are created using pre-defined operators CEA (2018). In the algorithm applied in this work, the equations were implemented in GIBIANE and were treated separately.

In this section, a parametric study inspired by Sercombe et al. Sercombe et al. (2001) is presented. The aim is to determine the influence of: thermal conductivity, the relationship between liquid saturation and humidity, intrinsic and relative liquid permeability on the problems results: temperature, liquid saturation, vapor pressure and mass loss.

5.2 Mesh, initial data and boundary conditions

All cases evaluated here were evaluated using the same mesh, initial data and boundary conditions.

The sensitivity analysis is carried for the heating of a cylindrical specimen ($\phi 110 \times h 220 \text{ mm}$). Considering symmetry characteristics, the proposed problem was solved using a quarter of the specimen section, which has the spatial discretization showed in Figure 1.

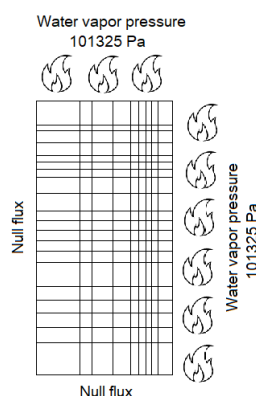


Figure 1: Geometry and boundary conditions used in the sensitivity analysis. 25×50 mesh, refined elements on the edges exposed to heating.

The specimen were subjected to temperatures ranging from $20^{\circ}C$ to $380^{\circ}C$, under a heating rate of $0.5^{\circ}C/min$. According to the geometry represented, this temperature evolution is imposed on upper and right edges, on the other two edges null flux was imposed. The initial liquid saturation is 46%, applied to the whole domain. The boundary condition for saturation is estimated in a way that the vapor pressure is constant and equal to ambient pressure. The initial porosity is $\phi_0 = 9.97\%$, and initial liquid intrinsic permeability is $K_0 = 2.4 \times 10^{-17} m^2$.

The concrete formulation considered is presented in Table 3.

5.3 Parameters adopted

The hygro-thermal model is applied for six different cases: the default or reference where all properties evolve normally, and the others, where a modification distinguished each case.

Constituent	Cement	Silico-calcareous aggregate	Water
Quantity (kg/m^3)	350	1950	150

Table 3: Sensitivity analysis - Concrete formulation.

- The first case studied was denominated Reference, in it all evolutions were used as proposed at Table 1.
- For the second case, here denominated λ_{60} , the concrete thermal conductivity was considered constant and equal to the one referent to the temperature of $60^\circ C$ ($\lambda_{60} = 1.28W/mK$).
- In the third case, denominated K_0 , the intrinsic permeability to gas was considered to be constant and equal to $K_0 = 2.4 \times 10^{-17}m^2$.
- In the fourth case, denominated k_{rl} , the liquid relative permeability was considered to be constant and equal to $k_{rl} = 0$.
- For the fifth case, denominated ϕ_0 , the porosity was considered to be constant and equal to the initial value adopted ($\phi_0 = 9.97\%$).
- In the last case, denominated $S_l(H_r)$, the parameter $\partial h_r / \partial S_l$ which was considered to be constant and equal to one, was then defined by an evolution based on Baroghel-Bouny (1994). The derivative $\partial h_r / \partial S_l$ weights on the evaluation of hydric conductivity ($D_h(S_l, d, T)$), Eq. (6) and is estimated using a linear approximation of the experimental curve. The derivative evolution is given in Table 4 and is compared to the reference case which considers that $h_r = S_l$, and consequently, $\partial h_r / \partial S_l = 1$.

S_l	0.08	0.17	0.22	0.3	0.4	0.5	0.61	0.72	0.83	0.9	0.95
$\partial h_r / \partial S_l$	0.6	2.6	2.2	1	1	0.8	0.8	0.7	1.1	1.2	0.8

Table 4: Humidity slope with respect to liquid saturation.

5.4 Results

Observing the mass loss evolution, shown in Figure 2, it is possible to see that heat conductivity variation (curve $\lambda = \lambda_{60}$), humidity-saturation relationship (curve $S_l = S_l(H_r)$) and porosity ($\phi = \phi_0$) almost don't affect the evolution of mass loss. It is only the variation of mass transfer parameters that create significative deviation: absence of liquid hydric transfer (curve $k_{rl} = 0$) and absence of intrinsic permeability to gas (curve $K = K_0$), which causes a smaller mass loss during the entire simulation.

Whereas only liquid hydric transfer is not taken into account (curve $k_{rl} = 0$), the mass loss evolution rate has two phases: one for temperatures below $100 - 150^\circ C$, in which the rate is smaller than the one for the reference case, and one for temperatures above $150^\circ C$, where the rate is larger. That shows the relevance of liquid hydric transfer for lowers temperatures. As for cases where capillarity effects are not considered, a three phases evolution is obtained: at the first a larger rate is associated to liquid water flow, at the second the rate is smaller, and at then the rate increases again.

The water vapor pressure results presented in Figure 3, shows that change at the porosity, thermal conductivity and liquid relative permeability kept constant, result in situations where

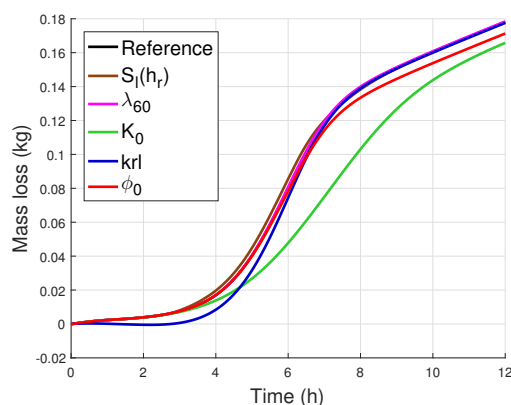


Figure 2: Mass loss with respect to time for various combinations of parameters.

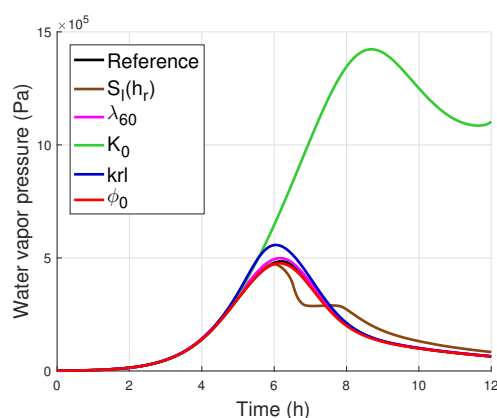


Figure 3: Water vapor pressure with respect to time for various combinations of parameters.

water vapor pressure almost don't deviate from the reference results. The parameters that cause larger alterations are associated to the absence of vapor intrinsic permeability and the shape of saturation-humidity curve. In the first case, the water vapor pressure peak is higher and delayed in regard to the reference case. About the saturation-humidity curve $Sl(Hr)$, the shape of the curve is different, there is a peak followed by a small level, and then returns to the reference's shape.

Regarding the water vapor pressure, the parameters that should impact the most are the intrinsic permeability to gas and the relative permeability to water, the smaller k_{rl} , more delimited is the dehydration front, and larger is the water vapor pressure peak. Also, it is concluded that only the data relative to water vapor intrinsic permeability are not enough to precisely estimate water vapor pressure during thermal transfer. An upper limit can be assessed, neglecting liquid water transfer. In that case, [Bazant and Kaplan \(1996\)](#) model is used. In it, water diffusion coefficient gains two orders of magnitude between $95^{\circ}C$ and $105^{\circ}C$, which leads to appearance of dehydration fronts and liquid saturation greater than 1 (due to dehydration of saturated zones).

A similar behavior is shown in [Figure 4](#): the thermal gradient peaks are more evident the smaller the relationship between intrinsic permeability to water and gas is. That is justified as a result of the vaporization of a bigger quantity of water in the center of the specimen, water which didn't or almost didn't migrate due to the liquid water gradient effect. The resulting hygro-thermal coupling (dehydration latent heat) it is even more pronounced (larger peaks and wavelength). The adoption of a constant value to vapor intrinsic permeability leads to, as for other results (mass loss, water vapor pressure), a time difference at the thermal gradient curve.

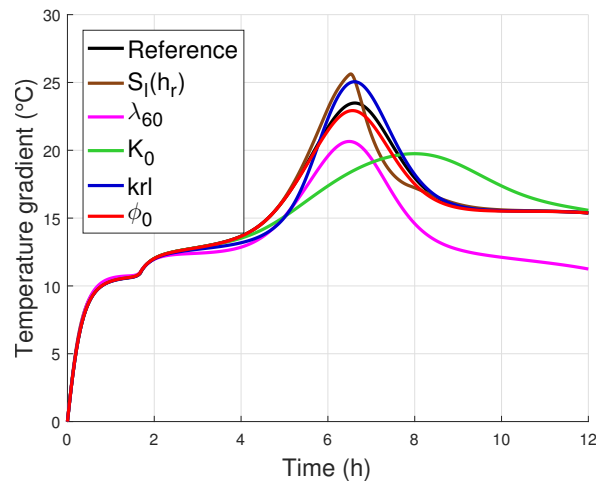


Figure 4: Temperature gradient with respect to time for various combinations of parameters.

Furthermore, the thermal gradient peak is even smaller, which can be explained by the uniformity of the liquid saturation field of the specimen (which leads to a slower mass loss) during heating, and consequently, a less remarkable vaporization. This result shows that the amplitude of thermal gradients is not necessarily related to water vapor pressure during thermal transitions.

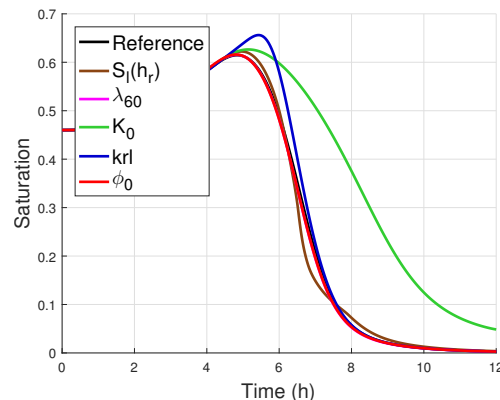


Figure 5: Liquid saturation with respect to time for various combinations of parameters.

The saturation results are shown in Figure 5, once more the curves highlighted are the ones regarding liquid relative permeability and water vapor intrinsic permeability, both of which affect directly the hydric transfer phenomena.

6 CONCLUSIONS

The present work consisted on the study of a hygro-thermal model applied to describe concrete structures behavior when subjected to high temperatures. In order to assess temperature, saturation and pressure distribution along the specimens, a numerical program applying a hygro-thermal implemented in an open access finite element code developed by the French Atomic Research Center (CEA) [CEA \(2018\)](#) was used.

The mathematical model is explained and a parametrical analysis is made due to the fact that the model require several properties to be defined, as shown in Table 1, which render important the need to determine which of them influence more the results. And thus, making it possible to simplify certain aspects and look into more accurate descriptions to increase the precision

of the results.

REFERENCES

- Baroghel-Bouny V. Caractérisation des pâtes de ciment et des bétons-méthodes, analyse, interprétation [characterization of cement pastes and concretes-methods, analysis, interpretations]. Technical Report, Technical report, Laboratoire Central des Ponts et Chaussées, Paris, France. In French, 1994.
- Bazant Z.P. and Kaplan M.F. *Concrete at high temperatures: material properties and mathematical models*. Longman, 1996.
- CEA. Site cast3m. <http://www-cast3m.cea.fr/>, 2018. Accessed: 2018-06-26.
- Chen D.P., Qian C.X., and Liu C.L. A numerical simulation approach to calculating hygro-thermal deformation of concrete based on heat and moisture transfer in porous medium. *International Journal of Civil Engineering*, 8(4):287–296, 2010.
- de Morais M.V.G., Noumowé A., Kanema M., Gallias J.L., and Cabrillac R. Transferts thermo-hydrauliques dans un élément en béton exposé à une température élevée: Approches numérique et expérimentale. *24ème Rencontres Universitaires de Génie Civil (AUGC06)*, pages 1–10, 2006.
- Ferreira A.P.G., Farage M.C., Barbosa F.S., Noumowé A., and Renault N. Thermo-hydric analysis of concrete-rock bilayers under fire conditions. *Engineering Structures*, 59:765–775, 2014.
- Gawin D., Majorana C.E., and Schrefler B.A. Numerical analysis of hygro-thermal behaviour and damage of concrete at high temperature. *Mechanics of Cohesive-frictional Materials*, 4(1):37–74, 1999. ISSN 1099-1484. doi:10.1002/(SICI)1099-1484(199901)4:1<37::AID-CFM58>3.0.CO;2-S.
- Gawin D., Pesavento F., and Schrefler B. Towards prediction of the thermal spalling risk through a multi-phase porous media model of concrete. *Computer Methods in Applied Mechanics and Engineering*, 195(41):5707 – 5729, 2006. ISSN 0045-7825. doi:https://doi.org/10.1016/j.cma.2005.10.021. John H. Argyris Memorial Issue. Part II.
- Kanema M., Noumowé A., Gallias J.L., and Cabrillac R. Influence of the mix parameters and microstructure on the behaviour of concrete at high temperature. In *Proceedings of 18th international conference on structural mechanics in reactor technology*. 2005.
- Khoury G.A. Effect of fire on concrete and concrete structures. *Progress in Structural Engineering and Materials*, 2(4):429–447, 2000. ISSN 1528-2716. doi:10.1002/pse.51.
- Mehta K. and Monteiro P. *Concrete Microstructure, Properties, and Materials*. Mc Graw Hill, 2006.
- Mindeguia J.C., Pimienta P., Noumowé A., and Kanema M. Temperature, pore pressure and mass variation of concrete subjected to high temperature — Experimental and numerical discussion on spalling risk. *Cement and Concrete Research*, 40(3):477–487, 2010.
- Sercombe J., Galle C., and Ranc G. Modélisation du comportement du béton à haute température: Transferts des fluides et de chaleur et déformations pendant les transitoires thermiques. *Note Technique SCCME*, 81, 2001.